

Nearly semi-elliptic relation between the minimal conductivity and Hall conductivity in unpaired Dirac fermions

Bo Fu,^{1,*} Kai-Zhi Bai,² Shi-Hao Bi,² and Shun-Qing Shen^{3,†}

¹*School of Sciences, Great Bay University, Dongguan 523000, China*

²*Department of Physics, The University of Hong Kong, Pokfulam Road, Hong Kong, China*

³*Department of Physics and State Key Laboratory of Optical Quantum Matter,
The University of Hong Kong, Pokfulam Road, Hong Kong, China*

(Dated: November 17, 2025)

Electric conductivities may reveal the topological and magnetic properties of band structures in solids, especially for two-dimensional unpaired Dirac fermions. In this work, we evaluate the longitudinal and Hall conductivity for unpaired Dirac fermions in the framework of the self-consistent Born approximation and find a nearly semi-elliptic relation between the minimal conductivity and Hall conductivities in the Dirac fermions. Near the charge neutrality point, disorder may drive a metal-insulator transition, and enhance the longitudinal conductivity. For the massless case, the minimal conductivity σ_{xx}^* coexists with the half-quantized Hall conductivity $\frac{e^2}{2h}$, forming an indicator for the parity anomalous semimetal. The relation signals a disorder-induced metallic phase that bridges two topologically distinct insulating phases, and agrees with the recent experimental observation in magnetic topological insulators.

Introduction. The interplay between topology and magnetism in electronic systems has unveiled a rich landscape of quantum phenomena [1–17]. A paramount achievement in this field is the quantum anomalous Hall effect (QAHE), a zero-magnetic-field state characterized by a quantized Hall conductance [18–24]. This state was first experimentally realized in magnetically doped topological insulator (TI) films, where the introduction of ferromagnetic order opens a gap in the Dirac surface states, revealing a topologically non-trivial ground state. The observation of the QAHE has since spurred intense research into its fundamental nature, particularly its connection to the more established integer quantum Hall effect (IQHE) in a strong magnetic field [23, 25]. A cornerstone of the IQHE theory is the universal scaling behavior of the longitudinal (σ_{xx}) and Hall (σ_{xy}) conductivities near critical points [26, 27]. Pioneering works demonstrated that the transition between IQHE plateaus follows a semicircle law in the $\sigma_{xy}-\sigma_{xx}$ plane, a relation that has been instrumental in analyzing critical transitions [28–31]. Recent experimental advances have enabled dynamic control of magnetization and the band gaps of the consequent surface states in a trilayer structures of V-doped (Bi, Se)₂Te₃ (V-BST)/(Bi, Se)₂Te₃ (BST)/ Cr-doped (Bi, Se)₂Te₃ (Cr-BST) [32, 33]. In these systems, the chemical potential can be precisely tuned to the charge neutrality point via gate voltage, accessing the Chern insulator, axion insulator [11, 34–37], and parity-anomalous semimetal (PAS) [38–40]. Intriguingly, these systems display diverse flow diagrams under in-plane and out-of-plane magnetic fields that deviates significantly from the conventional semicircle form. However, the fundamental origin of this flow diagram remains an open and critical question.

In this work, we evaluated the longitudinal and Hall conductivity for the Dirac fermions in the framework of the self-consistent Born approximation (SCBA), revealing that both

are governed by a single dimensionless parameter: the ratio between the mass-induced gap and the disorder broadening at charge neutrality point. This leads to a nearly semi-elliptic relation between σ_{xx} and σ_{xy} that specifically accounts for the unique properties of gapped Dirac fermion bands (in the unit of $\frac{e^2}{h}$, Fig. 1(b))

$$\left(\left| \sigma_{xy} \right| - \frac{1}{2} \right) - \sigma_c \Big)^2 + \frac{1}{(\pi\sigma_{xx}^*)^2} \left(\sigma_{xx} - \frac{\sigma_{xx}^*}{2} \right)^2 = \frac{1}{4\pi^2} \quad (1)$$

where $\sigma_c = \frac{1}{\pi} \arccos \sqrt{\sigma_{xx}/\sigma_{xx}^*}$ and its value is limited in the range of $0 \leq \sigma_c \leq \frac{1}{2}$. σ_{xx}^* is the minimal conductivity at $\sigma_{xy} = \pm \frac{e^2}{2h}$ for the massless Dirac fermions or parity anomalous semimetal. The point $(\sigma_{xx}, \sigma_{xy})$ traces a trajectory along this ellipse while the relevant parameters varies, demonstrating a universal scaling behavior of unpaired Dirac fermions. This scaling signals a disorder-induced critical metallic phase that bridges two topologically distinct insulating states [Fig. 1(a)]—a mechanism that fundamentally constrains the conductivities through the interplay of topology and disorder. Our theory, when applied to the TI sandwich heterostructure (Fig. 1(c)), quantitatively explains the characteristic two-stage anomalous flow observed under an in-plane magnetic field (Fig. 1(d)). This flow provides direct evidence for a parity-anomalous semimetal state. The model successfully reconciles theory with experiment by accounting for the diverse flow diagrams reported in recent studies.

Model Hamiltonian. To model the transport properties of the magnetic TI film, we construct an effective theory by projecting the full three-dimensional Hamiltonian onto the subspace spanned by the four lowest-energy bands related to the surface band [41, 42],

$$H_0 = \begin{pmatrix} H_t & M \\ M^\dagger & H_b \end{pmatrix}. \quad (2)$$

* fubo@gbu.edu.cn

† sshen@hku.hk

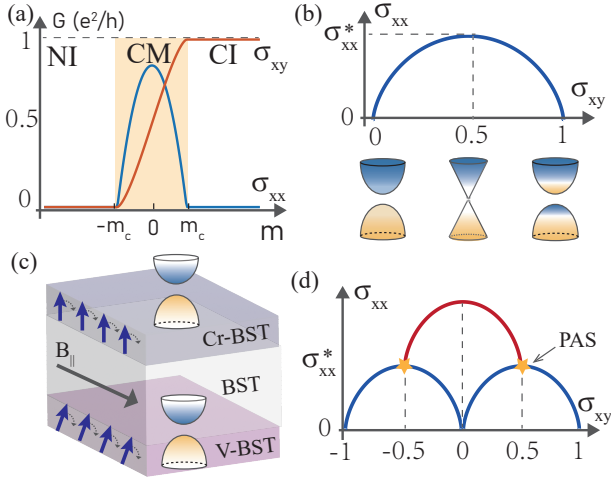


Figure 1. (a) The longitudinal (σ_{xx}) and Hall (σ_{xy}) conductivities at $E = 0$ as a function of the energy gap. The yellow-shaded region ($-m_c < m < m_c$) indicates an intermediate critical metallic (CM) phase, characterized by a non-quantized Hall conductivity and a non-zero σ_{xx} , which separates two insulating phases with distinct Chern numbers ($C = 0$ and $C = 1$). The critical mass $m_c = 2E_c e^{-1/2\gamma}$ depends on the disorder strength γ . The lower panel provides a schematic of the band inversion process, where the color gradient (blue to yellow) represents the sign of the Berry curvature. (b) Near semi-elliptical flow diagram of $(\sigma_{xy}, \sigma_{xx})$ based on Eq. (1), resulting from the formation of the intermediate metallic Hall phase. The peaks of the trajectory occur at $(\sigma_{xy}, \sigma_{xx}) = (\pm e^2/2h, \sigma_{xx}^*)$ which corresponds to a band gap closure. (c) Schematic of the heterostructure: a magnetic TI sandwich, with the top and bottom layers doped with Cr and V, respectively. The difference in coercive fields allows an in-plane magnetic field (B_{\parallel}) to independently switch the magnetic orientation of each layer, thereby directly tuning the band gap of the surface states. (d) Characteristic flow diagram for the magnetic TI sandwich under B_{\parallel} . The yellow pentangle indicates PAS.

Here, $H_{t/b}$ denote the Hamiltonians for the top (t) and bottom (b) surface states at low energies,

$$H_{t/b} = \hbar v(k_x \sigma_x + k_y \sigma_y) + m_{t/b} \sigma_z \quad (3)$$

where $m_{t/b}$ are the mass terms induced by an out-of-plane Zeeman field, and v is the Fermi velocity. The off-diagonal block M encodes the coupling between the two surface sub-blocks, which is significant only at high energies: $M(\mathbf{k}) = \Theta(bk^2 - m_0)(m_0 - b\mathbf{k}^2)\sigma_z$. Here $\Theta(x)$ denotes the Heaviside step function. The condition $m_0 b > 0$ is imposed to preserve the topological nature of three dimensional bulk. Consequently, within the momentum range $k < k_c = \sqrt{m_0/b}$, the coupling is identically zero ($M = 0$).

Self-consistent Born approximation and Insulator-Metal transition induced by disorder. To systematically treat the effects of quenched disorder, we employ the SCBA to evaluate the self energy. The disorder is modeled as a Gaussian white noise potential with the correlator: $\langle U_{\mathbf{k}-\mathbf{k}'} U_{\mathbf{k}'-\mathbf{k}} \rangle_{dis} = 4\pi\gamma(\hbar v)^2$ where γ is the dimensionless disorder strength. Within the SCBA framework, the self-energy $\Sigma(E, \mathbf{k})$, which renormalizes the electron's energy and lifetime, becomes

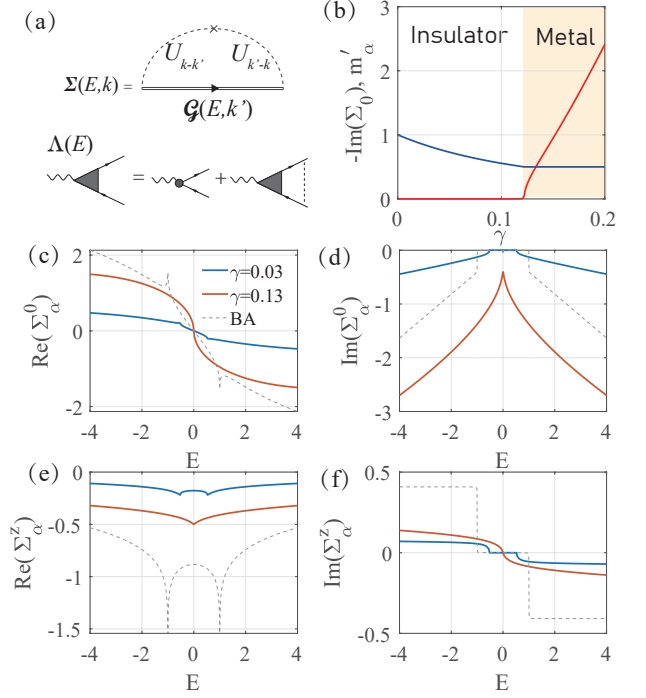


Figure 2. (a) Illustration of the Feynman diagram for the self-energy within the SCBA and vertex correction. (b) Imaginary part of the self-energy Σ_{α}^0 (red) and the renormalized gap m'_{α} (blue) as a function of disorder strength γ at zero energy. (c-f) Real and imaginary parts of the self-energies Σ_{α}^0 and Σ_{α}^z as a function of energy E for $\gamma = 0.03$ (below the critical disorder $\gamma_{\alpha,c}$) and $\gamma = 0.13$ (above $\gamma_{\alpha,c}$). Results from the Born approximation (BA, dashed lines) are shown for comparison. The bare gap $m_{\alpha} = 1$ is used as the energy unit.

momentum-independent. It is determined by the self-consistent equation, shown diagrammatically in Fig. 2(a) [43],

$$\Sigma_{\alpha}^{R/A}(E) = \left\langle \int \frac{d^2 \mathbf{k}'}{(2\pi)^2} U_{\mathbf{k}-\mathbf{k}'} \mathcal{G}_{\alpha}^{R/A}(E, \mathbf{k}') U_{\mathbf{k}'-\mathbf{k}} \right\rangle_{dis}, \quad (4)$$

where $\alpha = t, b$ and $\langle \dots \rangle_{dis}$ denotes the disorder-averaging. The corresponding retarded and advanced Green's functions for the subsystems are: $\mathcal{G}_{\alpha}^{R/A}(E, \mathbf{k}) = (E - \Sigma_{\alpha}^{R/A} - H_{\alpha})^{-1}$. The self-energy for gapped Dirac bands admits the decomposition $\Sigma_{\alpha} = \Sigma_{\alpha}^0 \sigma_0 + \Sigma_{\alpha}^z \sigma_z$. Substituting the corresponding Green's function into the self-energy equation and performing the momentum integration up to the high-energy cut-off $E_c \sim \hbar v k_c$, we obtain the following pair of self-consistent equations:

$$\Sigma_{\alpha}^0 = -\gamma(E - \Sigma_{\alpha}^0) \ln \left[\frac{-E_c^2}{(E - \Sigma_{\alpha}^0)^2 - (m_{\alpha} + \Sigma_{\alpha}^z)^2} \right]; \quad (5)$$

$$\Sigma_{\alpha}^z = -\gamma(m_{\alpha} + \Sigma_{\alpha}^z) \ln \left[\frac{-E_c^2}{(E - \Sigma_{\alpha}^0)^2 - (m_{\alpha} + \Sigma_{\alpha}^z)^2} \right]. \quad (6)$$

This set of equations can be solved numerically for the complex self-energy $\Sigma^{0,z} = \text{Re}\Sigma^{0,z} + i\text{Im}\Sigma^{0,z}$. Here, the real part $\text{Re}\Sigma^{0,z}$ describes energy renormalization and band gap

renormalization, respectively, and the imaginary parts $\text{Im}\Sigma^{0,z}$ characterizes the scattering rate and quasiparticle lifetime. At $E = 0$, the self-consistent equations simplify: Σ_α^0 becomes purely imaginary, while Σ_α^z becomes purely real. As shown in Fig. 2(b), Σ_α^0 is initially zero for weak disorder but becomes non-zero when γ exceeds a critical value, $\gamma_{\alpha,c} = \left(2 \ln \frac{2E_c}{|m_\alpha|}\right)^{-1}$. The retarded and advanced self-energies take the analytic form: $\Sigma_\alpha^{R/A} = \mp i \text{Re} \sqrt{E_c^2 e^{-1/\gamma} - (m_\alpha/2)^2}$. Concurrently, the renormalized mass parameter $m'_\alpha = m_\alpha + \Sigma_\alpha^z$ gradually decreases to $m_\alpha/2$ as γ approaches $\gamma_{\alpha,c}$ and remains constant thereafter. The density of states, given by $\nu_\alpha(E) = -\frac{1}{\pi} \int \frac{d^2\mathbf{k}}{(2\pi)^2} \text{ImTr}[\mathcal{G}_\alpha^R(E, \mathbf{k})]$ is directly related to the imaginary part of the self-energy Σ_α^0 , which can be expressed as $\nu_\alpha(E) = -\frac{\text{Im}\Sigma_\alpha^{0R}}{2\pi^2(\hbar v)^2\gamma}$. Within the SCBA, this implies that disorder can induce a phase transition from an insulating phase (topological or trivial) to a gapless metallic phase [44–46]. For a constant disorder strength γ , this transition occurs when the mass parameter m_α decreases to a critical value of $m_{\alpha,c} = 2E_c e^{-1/2\gamma}$. In the gapless case where $m_\alpha = 0$, the self-energy $\Sigma_\alpha^{R/A} = \mp i E_c e^{-1/2\gamma}$ remains finite for any infinitesimal disorder. The energy dependence of the self-energies Σ^0 and Σ^z is shown in Fig. 2(c-f) for disorder strengths below and above $\gamma_{\alpha,c}$. The real and imaginary parts exhibit opposite parity in energy, a consequence of the Kramers-Kronig relations. With increasing disorder, the band gap is gradually smeared, as evidenced by the broadening of the features in $\text{Im}\Sigma_\alpha^0$. Furthermore, the mass renormalization $\text{Re}\Sigma_\alpha^z$ is always negative, reducing the effective mass and thereby promoting the insulator-to-metal transition.

Charge Transport in Disordered Dirac Systems. The electrical conductivity tensor in the static limit can be evaluated from the Kubo formula. The SCBA framework allows us to extract essential physical parameters, including the renormalized energy $E'_\alpha = E - \Sigma_\alpha^{0R}$. Consequently, the zero-temperature conductivities for each subsystem can be obtained as

$$\sigma_{xx,\alpha} = \frac{1}{2\pi} \left(1 - \cos \phi_-^\alpha \left| \frac{\phi_+^\alpha}{\sin \phi_+^\alpha} \right| \right) \quad (7)$$

$$\sigma_{xy,\alpha} = \frac{1}{2\pi} \left(\phi_-^\alpha - \frac{\sin \phi_-^\alpha}{\sin \phi_+^\alpha} \phi_+^\alpha \right) + \sigma_{xy,\alpha}^* \quad (8)$$

where $\phi_+^\alpha = \text{Arg}(m_\alpha'^2 - E_\alpha'^2)$, $\phi_-^\alpha = \text{Arg}\left(\frac{m_\alpha' + E_\alpha'}{m_\alpha' - E_\alpha'}\right)$, and $\sigma_{xy,\alpha} = -\frac{1}{2} [\text{sgn}(m_\alpha) \pm \text{sgn}(b)]$ in which $\pm \frac{\text{sgn}(b)}{2}$ represents the contribution from the high-momentum regulator to ensure the cancellation of unphysical quantized values in the total Hall conductivity when the Fermi level lies within a gap [47]. The sign of this regulator term depends on whether the band is topologically trivial or nontrivial. Crucially, the regulator contributions for the two subsystems are always opposite in sign in this sandwich system.

The transport behavior governed by these expressions is illustrated in Fig. 3. Panel (a) shows the longitudinal conductivity $[\sigma_{xx,\alpha}(E)]$, which vanishes at the charge neutrality point ($E = 0$) below the critical disorder strength ($\gamma = 0.03$), reflecting the insulating state. Once γ exceeds $\gamma_{\alpha,c}$, a finite $\sigma_{xx,\alpha}$

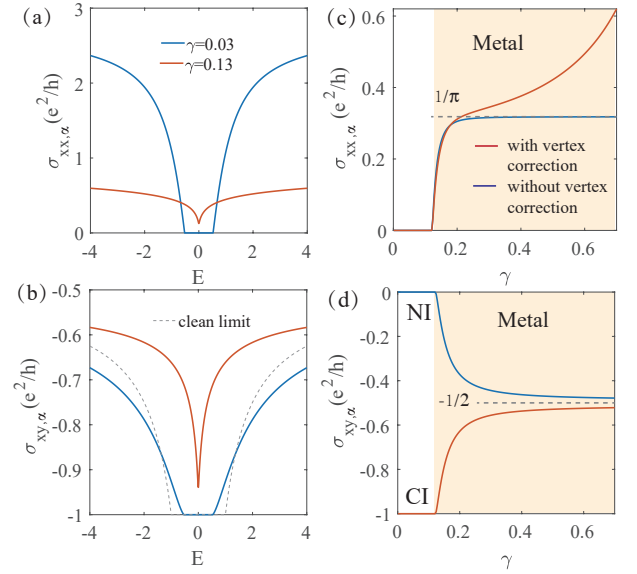


Figure 3. (a) Longitudinal conductivity ($\sigma_{xx,\alpha}$) and (b) Hall conductivity ($\sigma_{xy,\alpha}$) as a function of energy for two disorder strengths: $\gamma = 0.03$ (subcritical) and $\gamma = 0.13$ (supercritical). For reference, Hall conductivity in the clean-limit ($\gamma = 0$) is shown as a dashed line in (b). (c) The evolution of the zero-energy $\sigma_{xx,\alpha}$ with increasing disorder strength γ , calculated both with (red) and without (blue) vertex corrections. (d) Zero-energy Hall conductivity $\sigma_{xy,\alpha}$ as a function of γ for initial states of a normal insulator (NI, blue) and a Chern insulator (CI, red).

emerges at $E = 0$, signaling the breakdown of the insulating phase. Panel (b) displays the Hall conductivity $[\sigma_{xy,\alpha}(E)]$. For the subcritical disorder strength ($\gamma = 0.03$), $\sigma_{xy,\alpha}$ retains the characteristic plateau structure of the clean quantum Hall phase (dashed line) when the Fermi energy lies within the renormalized band gap. In contrast, for a supercritical disorder strength ($\gamma = 0.13$), these plateaus are washed out and the quantization is destroyed, a direct consequence of disorder-induced band broadening and gap closure. This transition is summarized in panels (c) and (d), which tracks the zero-energy ($E = 0$) conductivities as a function of γ . The rise of $\sigma_{xx,\alpha}$ and the simultaneous deviation of $\sigma_{xy,\alpha}$ from its quantized value at a critical $\gamma_{\alpha,c}$ provide direct transport signatures of the insulator-to-metal transition induced by disorder. For large disorder strengths, when the mass m_α is completely smeared, the system ultimately transitions to a parity anomalous semimetal state, characterized by $\sigma_{xx,\alpha} = \frac{e^2}{\pi h}$ and $\sigma_{xy,\alpha} = -\frac{e^2}{2h}$. Since the SCBA does not account for localization, our theory is expected to hold when the relevant spatial scales—such as the sample size L or the temperature-dependent phase-coherence length—are less than the localization length.

Conductivities at Charge Neutrality Point. For a finite chemical potential, the longitudinal and Hall conductivities are given by complex expressions involving the band gap m_α , the disorder broadening $\eta_\alpha = |\text{Im}\Sigma_{0,\alpha}^R|$, and the regulator parameter b . To isolate the universal behavior arising from the interplay between the band gap and disorder, we focus on the charge neutrality point ($E = 0$). At this point, the longitudinal con-

ductivity has the minimal value as the density of states reaches at the minimal when the chemical potential crosses the Dirac point. When $E \rightarrow 0$, one has $\text{Im}(\Sigma_\alpha^{zR}) \rightarrow 0$, and $\phi_+ \rightarrow 0$, $\phi_- \rightarrow 2 \arctan(\eta_\alpha/m'_\alpha)$. The only relevant energy scales are the gap m'_α and scattering induced broadening η_α , allowing us to define a single dimensionless parameter $\tilde{m}_\alpha = m'_\alpha/\eta_\alpha$. $\sin \phi_+/\phi_+ \rightarrow 1$ and $\cos \phi_- = (\tilde{m}_\alpha^2 - 1)/(1 + \tilde{m}_\alpha^2)$. Thus, in this regime, the conductivity formulas simplify significantly,

$$\sigma_{xx,\alpha} = \sigma_{xx,\alpha}^* \frac{1}{1 + \tilde{m}_\alpha^2}; \quad (9)$$

$$\sigma_{xy,\alpha} = \sigma_{xy,\alpha}^* + \frac{1}{\pi} \left(\arctan \frac{1}{\tilde{m}_\alpha} - \frac{\tilde{m}_\alpha}{1 + \tilde{m}_\alpha^2} \right). \quad (10)$$

In the weak scattering limit of $\tilde{m}_\alpha \rightarrow \infty$, $\sigma_{xx,\alpha} = 0$ and the Hall conductivity $\sigma_{xy,\alpha} = -\frac{\text{sgn}(\tilde{m}_\alpha) \pm \text{sgn}(b)}{2}$. It depends on the relative sign between the Dirac mass m_α and higher energy regulator b . In the massless limit of $\tilde{m}_\alpha \rightarrow 0$, $\sigma_{xy,\alpha} = \pm \frac{\text{sgn}(b)}{2}$ and $\sigma_{xx,\alpha} = \sigma_{xx,\alpha}^*$, which represents the minimal longitudinal conductivity at the charge neutrality point in the massless limit ($\tilde{m}_\alpha \rightarrow 0$). When fitting experimental data, $\sigma_{xx,\alpha}^*$ can be treated as a fitting parameter to account for realistic material-specific effects. By using the trigonometric function relations, we can remove the parameter \tilde{m}_α , and obtain the nearly semi-elliptic equation in Eq. (1), the main result of the present work. It is worth of stressing that the equation does not contain the point $(0, \pm 1/2)$, which means the Hall conductivity is not allowed to be non-integer in the insulating case.

Mechanisms for the Enhancement of $\sigma_{xx,\alpha}^$.* The measured $\sigma_{xx,\alpha}^*$ at the charge neutrality point in various systems are typically around $\sim 0.6 \frac{e^2}{h}$ at 20-30mK [14, 32, 33, 48]. The values are expected to decrease at even lower temperatures, but are still larger than $\frac{e^2}{\pi h}$ calculated by means of the SCBA [49]. This discrepancy might be related to a long-standing debate concerning the minimal conductivity of massless Dirac fermions in materials such as graphene and TIs. The different limiting procedures—specifically, the order in which the zero-frequency and zero-momentum limits are taken—yield distinct results, such as $\frac{e^2}{\pi h}$, $\frac{\pi e^2}{8h}$, or $\frac{\pi e^2}{4h}$ per valley per spin[50]. This non-universality is further complicated by scattering mechanisms. By incorporating the vertex corrections to the current operator [Fig. 2(a), bottom panel], we find that $\sigma_{xx,\alpha}^*$ is modified as: $\sigma_{xx,\alpha}^* = \frac{e^2}{\pi h} \frac{1}{1-\gamma^2}$ [51]. For a large scattering strength γ , this expression predicts a significant enhancement over the bare value of $\frac{e^2}{\pi h}$, as demonstrated in Fig. 3(c). Another possible contribution is the warping effect of the surface states in Be_2Te_3 [52, 53]. To account for the warping effects, we incorporate a term $\lambda(k_x^3 - 3k_x k_y^2) \sigma_z$ into $H_{t,b}$. $\sigma_{xx,\alpha}^*$ then depends on the dimensionless parameter $\tilde{\lambda} = \lambda(\text{Im}\Sigma_\alpha^{0R})^2/(\hbar v)^3$ and is enhanced beyond its bare value as $\tilde{\lambda}$ increases[51]. Furthermore, additional factors such as long-range disorder [54] and quantum interference effects can also elevate $\sigma_{xx,\alpha}^*$. A comprehensive theoretical resolution of this issue thus represents a significant and necessary challenge for future work.

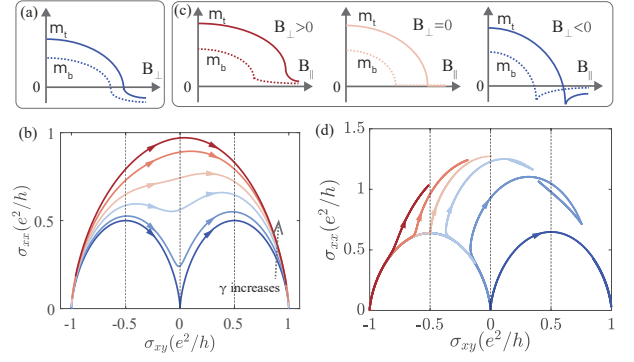


Figure 4. (a) Schematic of the mass terms $m_{t/b}$ in a magnetic TI sandwich as a function of perpendicular magnetic field B_\perp . (b) Corresponding theoretical flow diagrams in $(\sigma_{xy}, \sigma_{xx})$ plane. The color lines from blue to red traces the evolution from the weak to the strong scattering limit with increasing scattering strength γ . (c) Mass terms $m_{t/b}$ under an in-plane field B_\parallel for different fixed values of B_\perp : $B_\perp > 0$ (red), $= 0$ (orange), and < 0 (blue). (d) Resulting flow diagram under the application of B_\parallel .

Diverse Flow Diagrams in Trilayer systems. Consider the surface bands on distinct top and bottom surfaces ($\alpha = t, b$). The total Hall and longitudinal conductivities are the sum of contributions from both sectors. The resulting flow diagram of $(\sigma_{xy}, \sigma_{xx})$ in the parameter space depends critically on the external magnetic field, as summarized in Fig. 4. Using the Stoner-Wohlfarth model [55], we compute the mass terms $m_{t/b}$, respectively [51]. Fig. 4(a) illustrates how the Dirac mass on each surface varies with a perpendicular magnetic field (B_\perp) and in-plane magnetic field. We consider a scenario where the top and bottom surface masses change sign at two distinct critical fields B_\perp , creating an intermediate phase where the masses have opposite signs. The corresponding conductivity flow diagrams in Fig. 4(b) with the color gradient from blue to red traces the evolution from the weak to the strong scattering limit with increasing disorder strength γ . In the weak scattering limit (blue curve), where the disorder broadening is much smaller than the individual mass gaps, the trajectory of the flow forms a path comprised of two interconnected semi-elliptic segments that connect at the origin $(\sigma_{xy}, \sigma_{xx}) = (0, 0)$. In the strong scattering regime (red curve), significant disorder broadening smears out the intermediate axion insulator state, whose gap is relatively small. Consequently, the flow diagram collapses into a single, semi-elliptic curve connecting the two insulating states (e.g., from $\sigma_{xy} = +\frac{e^2}{h}$ to $\sigma_{xy} = -\frac{e^2}{h}$), with a single peak in σ_{xx} at the gap-closing point. At intermediate disorder strengths, the flow diagram exhibits a crossover between these two limiting behaviors. This framework provides a natural explanation for the measured flow diagrams in samples of varying thickness [51, 56].

Figure 4(c) illustrates the evolution of the mass terms under an in-plane field B_\parallel for different fixed values of B_\perp . The corresponding conductivity flow diagrams are shown in Fig. 4(d), with trajectories color-coded from red to blue as the fixed B_\perp value changes from positive to negative. For $B_\perp = 0$

, the distinct coercive fields cause the surface Zeeman fields to orient oppositely under B_{\parallel} , rendering one surface gapless ($m_b = 0$) while the other stays gapped ($m_t \neq 0$). The resulting conductivity flow [orange line in Fig. 4(d)] exhibits a distinct two-stage evolution: in the first stage, the system flows from its initial normal insulating state toward a PAS state characterized by a finite longitudinal conductivity and a half-quantized Hall conductivity; in the second stage, the net conductivity then follows an anomalous flow trajectory, which can be understood as the superposition of the conventional flow for a massive Dirac band and the constant background contribution from the established parity anomalous semimetal state. For fixed $B_{\perp} > 0$ (red line), both surfaces remain gapped, and the broken parity symmetry prevents the flow from reaching the half-quantized σ_{xy} point. For $B_{\perp} < 0$ (blue line), the B_{\parallel} -induced mass inversion leads to a flow resembling that of varying B_{\perp} . At large B_{\parallel} , both Zeeman fields are forced nearly in-plane, driving the system to a Dirac semimetal phase with $(\sigma_{xy}, \sigma_{xx}) = (0, 2\sigma_{xx}^*)$. Our theory provides excellent agreement with the experimental data obtained under in-plane magnetic fields [32, 51].

Discussion and Summary. The universal nearly semi-elliptic flow diagram discovered here for disordered massive Dirac fermions is fundamentally distinct from the semi-circle law of the IQHE. In our case, the fixed point at $(\sigma_{xy}, \sigma_{xx}) = (\pm \frac{e^2}{2h}, \sigma_{xx}^*)$ represents a PAS, where the half-quantized Hall conductivity is an intrinsic property of the gapless Dirac cone, arising from the topological Berry phase and coexisting with a finite minimal longitudinal conductivity. This is a direct manifestation of pristine Dirac physics in the presence of disorder. In stark contrast, the $\sigma_{xy} = \frac{e^2}{2h}$ point in the IQHE theory is not a stable phase but a critical point of the

localization transition, where a finite σ_{xx} arises solely from extended states inside the broadened Landau levels.

In this work, we discover a universal scaling law for topological transport: the longitudinal and Hall conductivities of disordered Dirac fermions at the charge neutrality point are constrained to a nearly semi-elliptic relation. This scaling trajectory, dictated by the interplay of topology and disorder, reveals that transitions between distinct insulating states are necessarily mediated by an intermediate metallic Hall phase. At the heart of this metallic phase lies the PAS, uniquely identified by the striking coexistence of the minimal longitudinal conductivity with the half-quantized Hall conductivity. This universal scaling framework quantitatively explains the enigmatic flow diagrams observed in various samples of magnetic TI sandwiches, thereby bridging a fundamental gap between theory and experiment in the landscape of topological quantum matter.

ACKNOWLEDGMENTS

This work was supported by the Quantum Science Center of Guangdong-Hong Kong-Macao Greater Bay Area (Grant No. GDZX230005) and the Research Grants Council, University Grants Committee, Hong Kong (Grants No. C7012-21G). B.F. is financially supported by National Natural Science Foundation of China (Grants No.12504049), Guangdong Province Introduced Innovative R&D Team Program (Grant No. 2023QN10X136), Guangdong Basic and Applied Basic Research Foundation (No. 2024A1515010430 and 2023A1515140008).

-
- [1] N. Nagaosa, J. Sinova, S. Onoda, A. H. MacDonald, and N. P. Ong, Anomalous Hall effect, *Rev. Mod. Phys.* **82**, 1539 (2010).
 - [2] D. Xiao, M.-C. Chang, and Q. Niu, Berry phase effects on electronic properties, *Rev. Mod. Phys.* **82**, 1959 (2010).
 - [3] K. Nomura and N. Nagaosa, Surface-Quantized Anomalous Hall Current and the Magnetoelectric Effect in Magnetically Disordered Topological Insulators, *Phys. Rev. Lett.* **106**, 166802 (2011).
 - [4] J. Wang, Q. Zhou, B. Lian, and S.-C. Zhang, Chiral topological superconductor and half-integer conductance plateau from quantum anomalous Hall plateau transition, *Phys. Rev. B* **92**, 064520 (2015).
 - [5] C.-X. Liu, S.-C. Zhang, and X.-L. Qi, The Quantum Anomalous Hall Effect: Theory and Experiment, *Annu. Rev. Condens. Matter Phys.* **7**, 301 (2016), <https://doi.org/10.1146/annurev-conmatphys-031115-011417>.
 - [6] S. Zhang, L. Pi, R. Wang, G. Yu, X.-C. Pan, Z. Wei, J. Zhang, C. Xi, Z. Bai, F. Fei, M. Wang, J. Liao, Y. Li, X. Wang, F. Song, Y. Zhang, B. Wang, D. Xing, and G. Wang, Anomalous quantization trajectory and parity anomaly in Co cluster decorated BiSbTeSe₂ nanodevices, *Nature Communications* **8** (2017), [10.1038/s41467-017-01065-7](https://doi.org/10.1038/s41467-017-01065-7).
 - [7] C.-X. Liu, X.-L. Qi, X. Dai, Z. Fang, and S.-C. Zhang, Quantum Anomalous Hall Effect in Hg_{1-y}Mn_yTe Quantum Wells, *Phys. Rev. Lett.* **101**, 146802 (2008).
 - [8] Z. Liu, G. Zhao, B. Liu, Z. F. Wang, J. Yang, and F. Liu, Intrinsic Quantum Anomalous Hall Effect with In-Plane Magnetization: Searching Rule and Material Prediction, *Phys. Rev. Lett.* **121**, 246401 (2018).
 - [9] M. Mogi, R. Yoshimi, A. Tsukazaki, K. Yasuda, Y. Kozuka, K. S. Takahashi, M. Kawasaki, and Y. Tokura, Magnetic modulation doping in topological insulators toward higher-temperature quantum anomalous Hall effect, *Applied Physics Letters* **107** (2015), [10.1063/1.4935075](https://doi.org/10.1063/1.4935075).
 - [10] P. Wang, J. Ge, J. Li, Y. Liu, Y. Xu, and J. Wang, Intrinsic magnetic topological insulators, *The Innovation* **2**, 100098 (2021).
 - [11] M. Mogi, M. Kawamura, R. Yoshimi, A. Tsukazaki, Y. Kozuka, N. Shirakawa, K. S. Takahashi, M. Kawasaki, and Y. Tokura, A magnetic heterostructure of topological insulators as a candidate for an axion insulator, *Nat. Mater.* **16**, 516 (2017).
 - [12] Y. Tokura, K. Yasuda, and A. Tsukazaki, Magnetic topological insulators, *Nat. Rev. Phys.* **1**, 126 (2019).
 - [13] H.-W. Wang, B. Fu, J.-Y. Zou, Z.-A. Hu, and S.-Q. Shen, Fractional electromagnetism response in a three-dimensional chiral anomalous semimetal, *Phys. Rev. B* **106**, 045111 (2022).
 - [14] M. Mogi, Y. Okamura, M. Kawamura, R. Yoshimi, K. Yasuda, A. Tsukazaki, K. Takahashi, T. Morimoto, N. Nagaosa, M. Kawasaki, *et al.*, Experimental Signature of the Parity

- Anomaly in a Semi-magnetic Topological Insulator, *Nature Physics* **18**, 390 (2022).
- [15] Z. Lu, T. Han, Y. Yao, A. P. Reddy, J. Yang, J. Seo, K. Watanabe, T. Taniguchi, L. Fu, and L. Ju, Fractional quantum anomalous Hall effect in multilayer graphene, *Nature* **626**, 759 (2024).
- [16] R. Lu, H. Sun, S. Kumar, Y. Wang, M. Gu, M. Zeng, Y.-J. Hao, J. Li, J. Shao, X.-M. Ma, Z. Hao, K. Zhang, W. Mansuer, J. Mei, Y. Zhao, C. Liu, K. Deng, W. Huang, B. Shen, K. Shimada, E. F. Schwier, C. Liu, Q. Liu, and C. Chen, Half-Magnetic Topological Insulator with Magnetization-Induced Dirac Gap at a Selected Surface, *Phys. Rev. X* **11**, 011039 (2021).
- [17] C.-Z. Chang, C.-X. Liu, and A. H. MacDonald, Colloquium: Quantum anomalous Hall effect, *Rev. Mod. Phys.* **95**, 011002 (2023).
- [18] D. J. Thouless, M. Kohmoto, M. P. Nightingale, and M. den Nijs, Quantized Hall Conductance in a Two-Dimensional Periodic Potential, *Phys. Rev. Lett.* **49**, 405 (1982).
- [19] F. D. M. Haldane, Model for a Quantum Hall Effect without Landau Levels: Condensed-Matter Realization of the “Parity Anomaly”, *Phys. Rev. Lett.* **61**, 2015 (1988).
- [20] R. Yu, W. Zhang, H.-J. Zhang, S.-C. Zhang, X. Dai, and Z. Fang, Quantized Anomalous Hall Effect in Magnetic Topological Insulators, *Science* **329**, 61 (2010).
- [21] R.-L. Chu, J. Shi, and S.-Q. Shen, Surface Edge State and Half-Quantized Hall Conductance in Topological Insulators, *Phys. Rev. B* **84**, 085312 (2011).
- [22] C.-Z. Chang, J. Zhang, X. Feng, J. Shen, Z. Zhang, M. Guo, K. Li, Y. Ou, P. Wei, L.-L. Wang, Z.-Q. Ji, Y. Feng, S. Ji, X. Chen, J. Jia, X. Dai, Z. Fang, S.-C. Zhang, K. He, Y. Wang, L. Lu, X.-C. Ma, and Q.-K. Xue, Experimental Observation of the Quantum Anomalous Hall Effect in a Magnetic Topological Insulator, *Science* **340**, 167 (2013).
- [23] J. G. Checkelsky, R. Yoshimi, A. Tsukazaki, K. S. Takahashi, Y. Kozuka, J. Falson, M. Kawasaki, and Y. Tokura, Trajectory of the anomalous Hall effect towards the quantized state in a ferromagnetic topological insulator, *Nat. Phys.* **10**, 731 (2014).
- [24] C.-Z. Chang, W. Zhao, D. Y. Kim, H. Zhang, B. A. Assaf, D. Heiman, S.-C. Zhang, C. Liu, M. H. W. Chan, and J. S. Moodera, High-precision realization of robust quantum anomalous Hall state in a hard ferromagnetic topological insulator, *Nat. Mater.* **14**, 473 (2015).
- [25] S. Grauer, K. M. Fijalkowski, S. Schreyeck, M. Winnerlein, K. Brunner, R. Thomale, C. Gould, and L. W. Molenkamp, Scaling of the Quantum Anomalous Hall Effect as an Indicator of Axion Electrodynamics, *Phys. Rev. Lett.* **118**, 246801 (2017).
- [26] B. Huckestein, Scaling theory of the integer quantum Hall effect, *Rev. Mod. Phys.* **67**, 357 (1995).
- [27] A. M. M. Pruisken, Universal Singularities in the Integral Quantum Hall Effect, *Phys. Rev. Lett.* **61**, 1297 (1988).
- [28] S. Kivelson, D.-H. Lee, and S.-C. Zhang, Global phase diagram in the quantum Hall effect, *Phys. Rev. B* **46**, 2223 (1992).
- [29] A. M. Dykhne and I. M. Ruzin, Theory of the fractional quantum Hall effect: The two-phase model, *Phys. Rev. B* **50**, 2369 (1994).
- [30] I. Ruzin and S. Feng, Universal Relation between Longitudinal and Transverse Conductivities in Quantum Hall Effect, *Phys. Rev. Lett.* **74**, 154 (1995).
- [31] B. P. Dolan, Modular invariance, universality and crossover in the quantum Hall effect, *Nucl. Phys. B* **554**, 487 (1999).
- [32] B. Wang, J. Hu, B. Fu, J. Li, Y. Kong, K.-Z. Bai, S.-Q. Shen, and D. Xiao, Parity Anomalous Semimetal with Minimal Conductivity Induced by an In-Plane Magnetic Field, arXiv preprint arXiv:2511.02446 (2025).
- [33] D. Zhuo, B. Zhang, H. Zhou, H. Tay, X. Liu, Z. Xi, C.-Z. Chen, and C.-Z. Chang, Evidence for Half-Quantized Chiral Edge Current in a $C=1/2$ Parity Anomaly State, arXiv preprint arXiv:2509.15525 (2025).
- [34] D. Zhang, M. Shi, T. Zhu, D. Xing, H. Zhang, and J. Wang, Topological Axion States in the Magnetic Insulator MnBi_2Te_4 with the Quantized Magnetoelectric Effect, *Phys. Rev. Lett.* **122**, 206401 (2019).
- [35] M. Mogi, M. Kawamura, A. Tsukazaki, R. Yoshimi, K. S. Takahashi, M. Kawasaki, and Y. Tokura, Tailoring tricolor structure of magnetic topological insulator for robust axion insulator, *Sci. Adv.* **3**, eaao1669 (2017).
- [36] D. Xiao, J. Jiang, J.-H. Shin, W. Wang, F. Wang, Y.-F. Zhao, C. Liu, W. Wu, M. H. W. Chan, N. Samarth, and C.-Z. Chang, Realization of the Axion Insulator State in Quantum Anomalous Hall Sandwich Heterostructures, *Phys. Rev. Lett.* **120**, 056801 (2018).
- [37] C. Liu, Y. Wang, H. Li, Y. Wu, Y. Li, J. Li, K. He, Y. Xu, J. Zhang, and Y. Wang, Robust axion insulator and Chern insulator phases in a two-dimensional antiferromagnetic topological insulator, *Nat. Mater.* **19**, 522 (2020).
- [38] B. Fu, J.-Y. Zou, Z.-A. Hu, H.-W. Wang, and S.-Q. Shen, Quantum Anomalous Semimetals, *npj Quantum Materials* **7**, 94 (2022).
- [39] J.-Y. Zou, B. Fu, H.-W. Wang, Z.-A. Hu, and S.-Q. Shen, Half-Quantized Hall Effect and Power Law Decay of Edge-Current Distribution, *Phys. Rev. B* **105**, L201106 (2022).
- [40] S.-Q. Shen, Half Quantized Hall Effect, *Coshare Science* **2**, 1 (2024).
- [41] J.-Y. Zou, R. Chen, B. Fu, H.-W. Wang, Z.-A. Hu, and S.-Q. Shen, Half-quantized Hall effect at the parity-invariant Fermi surface, *Phys. Rev. B* **107**, 125153 (2023).
- [42] K.-Z. Bai, B. Fu, and S.-Q. Shen, Dirac fermions and topological phases in magnetic topological insulator films, *SciPost Phys.* **17**, 146 (2024).
- [43] G. D. Mahan, “Nonzero temperatures,” in *Many-Particle Physics* (Springer US, Boston, MA, 2000) pp. 109–185.
- [44] J. S. Meyer and G. Refael, Disordered topological metals, *Phys. Rev. B* **87**, 104202 (2013).
- [45] S.-H. Bi, B. Fu, and S.-Q. Shen, Half-quantized Hall metal and marginal metal in disordered magnetic topological insulators, *Communications Physics* **8** (2025), 10.1038/s42005-025-02252-5.
- [46] S.-H. Bi, B. Fu, and S.-Q. Shen, Disordered parity anomalous semimetal, arXiv preprint arXiv:2408.11270 (2024).
- [47] H.-Z. Lu, W.-Y. Shan, W. Yao, Q. Niu, and S.-Q. Shen, Massive Dirac fermions and spin physics in an ultrathin film of topological insulator, *Phys. Rev. B* **81**, 115407 (2010).
- [48] T.-H. Yang, Y. Li, P. Zhang, Y.-T. Yao, H.-Y. Yang, Q. Shu, E. S. Choi, K. Wong, T.-R. Chang, G. Qiu, and K. L. Wang, In-plane field induced half quantized Hall conductivity in trilayer magnetic topological insulator, *Advanced Materials* (2025).
- [49] P. M. Ostrovsky, I. V. Gornyi, and A. D. Mirlin, Electron transport in disordered graphene, *Phys. Rev. B* **74**, 235443 (2006).
- [50] K. Ziegler, Minimal conductivity of graphene: Nonuniversal values from the Kubo formula, *Phys. Rev. B* **75**, 233407 (2007).
- [51] See Supplemental Material at [URL to be added by publisher] for details of (Sec. S1) Vertex Correction to the Minimal Conductivity; (Sec. S2) Warping-Induced Modifications of Minimal Conductivity σ_{xx}^* ; (Sec. S3) Surface Magnetism from Stoner-Wohlfarth Model; and (Sec. S4) Experimental-theoretical comparison of flow diagrams in magnetic topological insulator sandwiches, which includes Refs. [32, 33, 52, 56].
- [52] L. Fu, Hexagonal Warping Effects in the Surface States of the Topological Insulator Bi_2Te_3 , *Phys. Rev. Lett.* **103**, 266801 (2009).

- [53] J. Cserti, A. Csordás, and G. Dávid, Role of the Trigonal Warping on the Minimal Conductivity of Bilayer Graphene, *Phys. Rev. Lett.* **99**, 066802 (2007).
- [54] W. Chen, Y. Shen, B. Fu, Q. Shi, and W. Zhu, Origin of minimal conductivity in Dirac materials: Momentum-dependent self-energy function from long-ranged disorder scattering, *Phys. Rev. B* **108**, 174205 (2023).
- [55] C. Tannous and J. Gieraltowski, The Stoner–Wohlfarth model of ferromagnetism, *Eur. J. Phys* **29**, 475 (2008).
- [56] R. Zhang, Y.-F. Zhao, L.-J. Zhou, D. Zhuo, Z.-J. Yan, C.-X. Liu, M. H. W. Chan, C.-Z. Chen, and C.-Z. Chang, Interlayer exchange coupling induced critical-metal-to-insulator phase transition in quantum anomalous Hall insulators, *Phys. Rev. B* **112**, 125402 (2025).